

Interference with correlated photons: Five quantum mechanics experiments for undergraduates

E. J. Galvez, C. H. Holbrow, M. J. Pysher, J. W. Martin, N. Courtemanche, L. Heilig, and J. Spencer

Department of Physics and Astronomy, Colgate University, Hamilton, New York 13346

(Received 15 March 2004; accepted 29 July 2004)

We describe five quantum mechanics experiments that have been designed for an undergraduate setting. The experiments use correlated photons produced by parametric down conversion to generate interference patterns in interferometers. The photons are counted individually. The experimental results illustrate the consequences of multiple paths, indistinguishability, and entanglement. We analyze the results quantitatively using plane-wave probability amplitudes combined according to Feynman's rules, the state-vector formalism, and amplitude packets. The apparatus fits on a 2'×4' optical breadboard. © 2005 American Association of Physics Teachers. [DOI: 10.1119/1.1796811]

I. INTRODUCTION

Advances in laboratory techniques for doing experiments with single photons have stimulated studies of the fundamentals of quantum mechanics that underlie such interesting applications as quantum cryptography and quantum computing.¹ In particular, the ability to produce pairs of correlated photons allows us to bring beautiful laboratory demonstrations of quantum superposition to an undergraduate setting where simplicity and affordability are primary concerns.²

In this article we describe five table-top experiments that involve the interference of photons detected by a counting apparatus. The experiments involve photons passing through an interferometer, where alternative paths can be made distinguishable or indistinguishable. These experiments can provide the basis for an undergraduate laboratory on the fundamentals of quantum mechanics as proposed in Ref. 3. They go beyond transforming interferometer fringes into counter clicks and challenge classical intuition with results that are unquestionably nonclassical. By incorporating these experiments into undergraduate quantum mechanics instruction, we hope to encourage students to discuss and consider the consequences of quantum mechanical superposition such as entanglement and nonlocality.

The experiments have the attractive feature that their results can be analyzed and understood by undergraduates. We try to explain them in ways that we believe will be useful and accessible to them. Our explanations assume that they are acquainted with the basic ideas of interference and wave packets and that they have learned, or can quickly learn, to use the complex exponential representation of plane waves—what Feynman ingeniously described as “clock numbers.”⁴

The first of the five experiments demonstrates that a photon interferes with itself when it can reach a detector by either of two indistinguishable paths. We observe this effect by changing the phase of one of the paths without making the paths distinguishable. We also show what happens to the interference pattern when, using filters and other optical elements, we modify the extent to which the two paths are indistinguishable. In the second experiment we pass an entangled pair of photons through an interferometer and observe and analyze the unusual interference properties of this biphoton. In the third experiment, we create photons in po-

larization states and manipulate these states as examples of the formation, projection, and transformation of quantum states. We also cause the interference pattern to disappear by manipulating the polarization states of the photons to make the paths through the interferometer distinguishable. A fourth experiment, the quantum eraser, demonstrates how interference can be made manifest in subsets of events that together exhibit no interference. Finally, we perform a conceptually simple experiment that can show that the photon does not split.

Most of our experiments and layouts are based on published landmark experiments on the fundamentals of quantum mechanics. Our references show the sources that we consulted, but they are not chronological or comprehensive.

The cost of the experiments ranges from \$14,000 to \$35,000 depending on the equipment at hand. The cost is dominated by the price of a blue laser (\$2000–\$6000) and two avalanche photodiode detectors (\$4000 each). These prices are likely to decrease in the near future as the technologies mature. The cost of the remaining items depends on the availability of optical hardware and conventional electronics. In Appendix A we list vendors and the prices of the components.

II. APPARATUS

A. The laser

At the heart of the experiments is the production of a pair of photons by spontaneous parametric down conversion, a nonlinear effect that produces two photons from one pump photon.⁵ For historical reasons the two outgoing photons are usually called the “idler” and the “signal” photon. We use the subscripts p , i , and s to refer to the pump, idler, and signal photons, respectively. Conservation of energy requires that

$$E_p = E_s + E_i, \quad (1)$$

where E_p is the energy of the pump photon, and E_s and E_i are the energies of the down-conversion photons. It is often convenient to use the alternative forms of Eq. (1),

$$\omega_p = \omega_i + \omega_s, \quad (2a)$$

$$k_p = k_i + k_s, \quad (2b)$$

$$\frac{1}{\lambda_p} = \frac{1}{\lambda_i} + \frac{1}{\lambda_s}, \quad (2c)$$

which are based on the fact that $E = \hbar\omega = \hbar kc = hc/\lambda$ for a photon, where ω is the angular frequency of the light and k is the magnitude of its wave number in vacuum. The wave number k is related to the wavelength in vacuum λ by $k = 2\pi/\lambda = \omega/c$, where c is the speed of light.

High detection efficiency of down-conversion photons is essential for our experiments and severely limits the choice of pump laser. Efficiency is important because our experiments depend on selecting down-conversion pairs of photons from the background. We select the photon pairs by detecting them in coincidence, making use of the fact that two down-conversion photons always are produced at nearly the same time. Because the efficiency of coincidence detection is the product of the individual detector efficiencies, it is necessary to use the most efficient single-photon detectors available. These are avalanche photodiodes. Their efficiencies peak at around 80% for 700 nm photons and drop off rather quickly to below 10% for 1000 nm photons.⁶ Because detection efficiencies vary strongly with wavelength, we concentrate on the case where $k_s = k_i = k_p/2$.

To operate detectors at their peak efficiency, we want down-conversion photons with wavelengths of about 700 nm. To obtain these photons, the best pump laser is an expensive UV argon-ion laser operated at 351.1 nm, which is widely used for research. For this wavelength there currently are no less expensive alternatives. We used two compromises: an 18 mW, 402.36 nm GaN diode laser and a 100 mW, 457.9 nm argon-ion laser. The GaN laser has become the choice of the compact-disk industry for data storage at higher resolution, so its price is likely to go down.⁷ Avalanche photodiodes have an efficiency of about 60% at 804.72 nm. The 457.9 nm line was the shortest wavelength available to us from an old multiline argon-ion laser that had been used for pumping a cw dye laser. The avalanche photodiodes efficiency for the 915.8 nm down-conversion photons is 30%.

B. The crystal

The argon-ion laser produces a near-IR background glow that needs to be removed, so it is common to use either a dispersing prism or a dielectric mirror between the pump and the down-converter crystal. We used both in the two experimental setups reported here. In both cases we arranged for the polarization of the pump beam to be horizontal. The output of the argon laser was vertically polarized, so we rotated it using mirrors.⁸ Standard laser safety precautions should be used when steering the laser into the crystal.

We used nonlinear crystals cut for type-I parametric down-conversion to produce a pair of down-conversion photons with linear polarizations parallel to each other but orthogonal to the polarization of the pump beam (see Appendix B). We set up the beta-barium-borate down-conversion crystals (5–7 mm thick) in the arrangements shown schematically in Fig. 1. In Fig. 1(a) the pairs of down-conversion photons leave the crystal at $\pm 3^\circ$ to the pump-beam axis; for the arrangement in Fig. 1(b) they left at 0° (that is, they were collinear). In addition to energy conservation (see Eq. (1)), parametric down-conversion requires that the photon momentum \mathbf{p} is conserved inside the crystal. The momentum is related to the wave vector by the relation $\mathbf{p} = \hbar \mathbf{k}$. The wave number inside

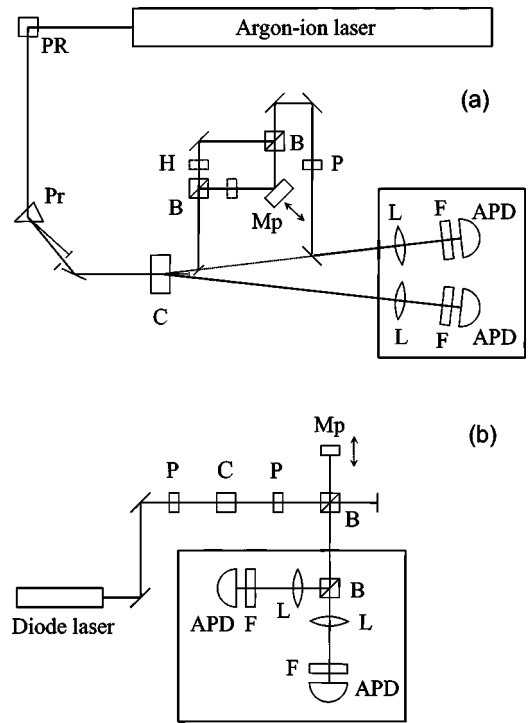


Fig. 1. In (a) the down-conversion photons travel separate paths; in (b) they travel the same paths. The optical components are polarization rotator (PR), prism (Pr), down-converter crystal (C), nonpolarizing 50-50 beam splitter (B), half-wave plate (H), polarizer (P), mirror moved by a piezoelectric stack (Mp), lens (L), bandpass filter (F), and avalanche photodiode (APD).

the crystal is $|\mathbf{k}| = nk = 2\pi n/\lambda$, with n being the index of refraction of the crystal. This momentum conservation condition can be expressed in terms of the wave vectors as

$$\mathbf{k}_p = \mathbf{k}_s + \mathbf{k}_i. \quad (3)$$

The directions taken by the down-conversion photons of specific but complementary wavelengths are determined by the angle formed by the optic axis of the crystal (OA) and the propagation direction of the pump beam, the phase-matching angle θ_m . As described in Appendix B, the down conversion of 457.9 nm into 915.8 nm at $\pm 3^\circ$ requires $\theta_m = 26.13^\circ$. Similarly, $\theta_m = 29.01^\circ$ is required for down conversion of 402.36 nm into 804.72 nm at 0° . The crystals were mounted on a rotation stage so that OA was in a horizontal plane. In this way we could easily fine tune the phase-matching angle of the crystal.

C. The detectors

We chose avalanche photodiodes modules optimized for high quantum efficiency and configured to output TTL pulses, suitable for the electronics that we had available.

In the setup of Fig. 1(a) one down-conversion photon, the idler, was sent directly to a detector, while the other photon, the signal, was sent through a Mach-Zehnder interferometer to a second detector. Only coincidences of the TTL output of both detectors were recorded. In effect the idler tags the signal photon, but in reality the photons are much more intimately connected, because their wave functions are entangled as we will discuss. In the setup of Fig. 1(b) there is no distinction between idler and signal, because both photons can travel the same path. In this case we place a beam splitter

at the interferometer's output and look for coincidences between photons emerging from separate outputs of this beam splitter.

It is very important to keep the avalanche photodiodes from receiving ambient light, because they can be destroyed by excess photons. To avoid doing the experiments in complete darkness, we put the detector pair of each setup inside a light-tight box made of an aluminum frame and black poster-board walls. The down-conversion photons enter the detector boxes through windows covered by red filters. The protective boxes allowed us to illuminate the work area with low-level illumination from blue LEDs. Each avalanche photodiode had a short focal length lens (40–100 mm) to focus the light onto the small active area of the avalanche photodiode (0.175 mm diameter). A narrow-band filter (10 nm, 1 nm, or 0.1 nm) prevented the avalanche photodiodes from being overwhelmed by photons that were not in the wavelength region of interest. The filters also served to determine the bandwidth of the detected light, as described in Sec. III.

D. The electronics

We used NIM electronics (nuclear instrument modules) to perform coincidence detection of the TTL pulses from the avalanche photodiodes. The minimum electronics required are counters and coincidence modules. Because the signal and idler photons traveled different distances to reach the detectors, we used a time-to-amplitude converter (TAC), a single channel analyzer (SCA), and a multichannel scaler to register coincident events. Manipulating the beams so that both photons travel the same distance would reduce the amount of electronics required,² but it would have unacceptably increased the constraints on our optical layout.

We used a combined TAC/SCA unit (Canberra model 2145), which had both TAC and SCA outputs. The pulses from the signal detector passed through an extra three meters of cable deliberately inserted to produce a 15 ns delay between the pulses produced by the detection of the signal and idler photons. The idler and the signal pulses were sent to the start and stop inputs of the TAC/SCA, respectively. The TAC output was sent to the multichannel scaler for pulse-height analysis. The output of the multichannel scaler consisted of a histogram of the number of pairs of pulses as a function of the time delay between them. We used three counters, two to register the (singles) counts from each detector and one to record the SCA output, that is, the coincidences. After a year of operation, we automated the data acquisition using Labview⁹ and shortened the data acquisition time from hours to minutes.

E. First steps

Our experimental setups were designed to take into account that the down-conversion beams are too weak to be seen. Down-conversion efficiencies at the wavelength of interest are typically about 10^{-10} . Therefore, it is necessary to prealign the optical components and detectors, and, of course, any interferometer. Prealignment requires a very methodical approach: calculating the positions of the detectors, setting up irises, and tracing the expected path of the down-converted beam with the beam from a HeNe laser. The other requirement is flexibility: the crystal is mounted on a rotation stage that permits fine tuning of the phase-matching angle, and the lens in front of each avalanche photodiode is ar-

ranged to be displaced transversely in order to fine-steer the focused light onto the small photodetector area.

These techniques are very useful to obtain the first signals. We start by maximizing the singles counts on each detector (expecting 10–100 kHz) by varying the position of the lens in front of each detector. Then we set the TAC/SCA to record photon pairs delayed by a time in the range 0–50 ns and look for a peak in the multichannel scaler output around a 15 ns delay. When the optical layout is aligned properly, there is a prominent peak at that delay representing the down-conversion pair. Once the signal is obtained, we narrow the TAC/SCA window to about 4 ns centered around the down-conversion peak. The SCA output then represents down-conversion events. If the TAC and SCA are separate modules, the voltage window of the SCA determines the time window.

F. Interferometers

We used both Mach–Zehnder and Michelson interferometers. The former is more elegant but requires more optical elements and greater care in setting up. To align it we started with a pilot beam from a HeNe laser and put each of the interferometer components (that is, mirrors and beam splitters) into place one by one. We used irises to align the beams parallel to the holes of the breadboard.⁹ In the arrangement of Fig. 1(a) we set up the interferometer so that we could optimize the down-conversion and the interferometry separately. Because stability is important, we linked all the mounting posts in the interferometers to each other by 1/2" diameter rods (Invar or stainless steel). We also were able to find adequate stability by using short pedestal mounts for the optics instead of posts with rod links. We mounted one of the mirrors on a translation stage to be able to adjust the difference between the path lengths of the interferometer's arms to near zero, that is, the point where white-light fringes are observed.⁹ This adjustment was needed because the coherence of the down-converted light is limited. Indeed, adjusting the stage to increase the path difference to somewhat less than 1 mm caused the fringes to disappear.

Our experiments were done by slightly varying the difference between the lengths of the arms of the interferometer by moving one of the interferometer mirrors with a stack of piezoelectric transducers either glued directly to the mirror and mirror mount or placed as a spacer in the translation stage where the mirror was mounted. The piezo had a response of about 40 nm/V. When our setup was automated, the output of a digital-to-analog interface was fed to a high-voltage amplifier to scan the voltage on the piezo.

III. ONE-PHOTON INTERFERENCE

The probability amplitude, a complex number, is a key idea in quantum mechanics. Interference arises from squaring the sum of the probability amplitudes for alternative ways to the same observational outcome. Interference can occur if two or more different ways to produce the same result cannot be distinguished with the apparatus. If the apparatus yields information that can distinguish between alternatives, interference will not occur.

Feynman states the conditions for interference in three rules:¹⁰ (1) the probability P of a particular outcome from the interaction of a particle with an apparatus is given by the square of the absolute value of a complex probability amplitude ϕ : $P = |\phi|^2$; (2) when the same outcome can occur in

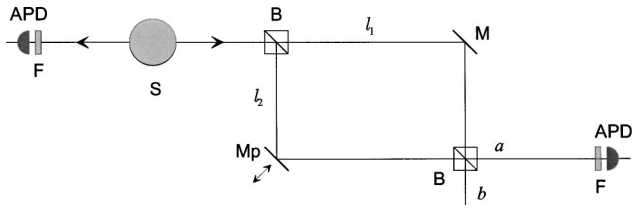


Fig. 2. Schematic of the experiments using a Mach–Zehnder interferometer. The labeled components shown are source of down converted photons (S), nonpolarizing 50-50 beam splitter (B), mirror moved by a piezoelectric stack (Mp), lens (L), bandpass filter (F), and avalanche photodiode. The interferometer arms have lengths ℓ_1 and ℓ_2 , and its output ports are labeled a and b .

indistinguishable alternative ways, the probability amplitude is the sum of the probability amplitudes for each way considered separately: $P = |\phi_1 + \phi_2|^2$; (3) when an experiment is performed that is capable of determining which way the outcome occurred, the probability of the outcome is the sum of the probabilities of each alternative: $P = P_1 + P_2 = |\phi_1|^2 + |\phi_2|^2$.

Although Feynman’s approach describes how basic interference patterns arise, a more complete theory is needed to explain partial interference and to give students insight into the coincidence detection of photons.

A. One-photon interference pattern: Prediction

Feynman’s approach can predict the interference pattern produced by an interferometer with nearly equal arm lengths because the resulting interference pattern is insensitive to the details of the amplitudes.¹¹ We can assume the amplitudes are plane waves modified by reflection and transmission at the beam splitter as the photons pass through the setup of Fig. 2. At the first beam splitter a photon has two possible outcomes: either transmission with an amplitude t into arm 1 or reflection with amplitude r into arm 2. The plane wave associated with path $j=1,2$ acquires a phase $\delta_j = k_s \ell_j$, where ℓ_j is the length of arm j and $k_s = 2\pi/\lambda_s$ is the wave number of the signal photon.¹² Therefore the probability amplitude for emerging from path 1 is $tre^{i\delta_1}$ and that from path 2 is $rte^{i\delta_2}$.

The probability P that a photon will be detected at the a port of the second beam splitter (see Fig. 2) is the square of the modulus of the sum of these two amplitudes:

$$P = |tre^{i\delta_1} + rte^{i\delta_2}|^2 \quad (4a)$$

$$= rr^* tt^* [2 + e^{i(\delta_1 - \delta_2)} + e^{-i(\delta_1 - \delta_2)}] \quad (4b)$$

$$= 2RT[1 + \cos \delta], \quad (4c)$$

where $R = rr^*$ and $T = tt^*$ are the reflection and transmission probabilities, respectively, and $\delta = \delta_1 - \delta_2$ is the phase difference arising from the difference between lengths of the two arms of the interferometer. We assume the beam splitters are identical and symmetric.³ For the common case of a 50-50 beam splitter, $R = 1/2$ and $T = 1/2$, and Eq. (4c) becomes $P = 1/2(1 + \cos \delta)$. This result implies that varying δ will produce a variation in the number of photons emerging from the interferometer, that is, there will be an interference pattern.

To introduce bra and ket notation for state vectors, we could use the slightly more sophisticated explanation offered by Greenberger, Horne, and Zeilinger.¹³ A photon in a state

$|s\rangle$ enters the Mach–Zehnder interferometer and interacts with the first beam splitter. The beam splitter transforms the state of the input photon into

$$|s\rangle = t|\ell_1\rangle + r|\ell_2\rangle, \quad (5)$$

where $|\ell_1\rangle$ and $|\ell_2\rangle$ refer to the states of the photon in the interferometer arms. If $|a\rangle$ and $|b\rangle$ denote the state of the signal photon exiting the a and b output ports of the interferometer, respectively, then

$$|\ell_1\rangle = e^{i\delta_1}(r|a\rangle + t|b\rangle), \quad (6a)$$

$$|\ell_2\rangle = e^{i\delta_2}(t|a\rangle + r|b\rangle). \quad (6b)$$

We combine Eqs. (5)–(6b) and express the overall transformation of $|s\rangle$ as

$$|s\rangle = rt(e^{i\delta_1} + e^{i\delta_2})|a\rangle + (tte^{i\delta_1} + rre^{i\delta_2})|b\rangle. \quad (7)$$

The interference pattern arises from the probability of detecting a photon in state $|a\rangle$,

$$P(\delta) = |\langle a|s\rangle|^2 = 2RT(1 + \cos \delta). \quad (8)$$

Equation (8) is the same result as Eq. (4c) with the desirable feature that the formalism conveniently yields the amplitude for a photon to arrive at the other output, that is, in state $|b\rangle$.¹⁴

B. One-photon interference: Experimental results

To be sure we were measuring an interference pattern produced by individual photons, we used coincidences between down-conversion pairs. We recorded the detection of a signal photon at output a of the interferometer only when an idler photon was detected at another detector. Thus each down-conversion signal photon passing through the interferometer was tagged by its idler companion. Such a tagging procedure does not change the expected interference pattern, because the crystal down converts a pump photon $|p\rangle$ into a pair of states $|p\rangle \rightarrow \eta|i\rangle|s\rangle$, where η , the amplitude for down conversion into a signal and an idler photon, $|s\rangle$ and $|i\rangle$, is the order of 10^{-5} or 10^{-6} . The effect is to multiply all the terms in Eq. (7) by $\eta|i\rangle$, which does not introduce any additional relative phase shift. As a result, the overall probability remains proportional to Eq. (8) although the count rate will drop by 10^{-10} or so.¹⁵

The interferometer was set up to make its arm lengths as closely equal as possible, that is, $|\ell_1 - \ell_2| = \Delta\ell \sim 0$, by aligning it to produce white-light fringes. Then with 10 nm bandpass filters centered on the down-conversion wavelength in front of both detectors, we obtained the interference fringes in the coincidence counts N_c shown in Fig. 3(a). The data are the number of recorded coincidences as a function of δ , which was varied by changing ℓ_2 via the piezo-driven mirror in the interferometer arm (Mp in Fig. 1). The error bars are proportional to \sqrt{N} , due to Poisson statistics. The slight horizontal deformation of the sinusoid is a reflection of the nonlinear relation between the displacement of the piezo and the voltage applied to it.

The data were corrected for accidental coincidences. These arise from the accidental simultaneous arrival of two unrelated photons. The number of these events is estimated from the relation

$$N_{\text{acc}} = N_s N_i \Delta T, \quad (9)$$

where N_s and N_i are the singles counts at the signal and the idler detectors respectively, and ΔT is the width of the coin-

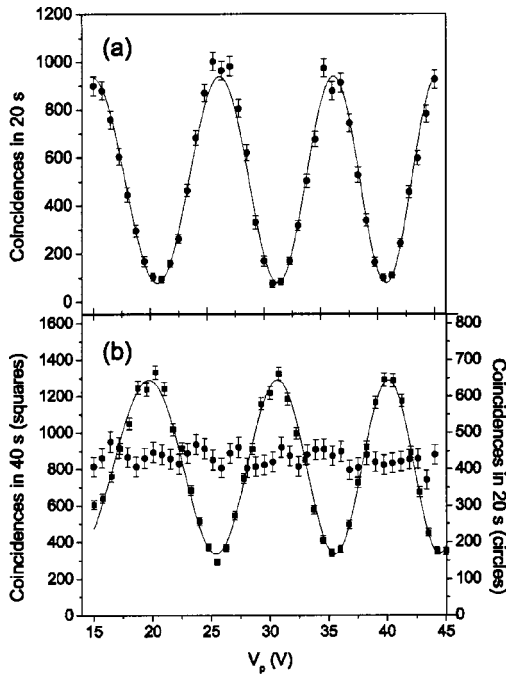


Fig. 3. Coincidence counts as a function of the voltage on the piezoelectric stack used to change the interferometer path-length difference $\Delta\ell$. The data in (a) and (b) correspond to $\Delta\ell \sim 0$ and $\Delta\ell \sim 144 \mu\text{m}$, respectively. For the circles both detectors had 10 nm bandpass filters in front of them. The squares in (b) correspond to having a 10 nm filter in front of the signal detector and a 0.1 nm filter in front of the idler detector.

cidence window set by the TAC/SCA. The time window was $\Delta T = 4 \text{ ns}$. For the experiment of Fig. 3(a), $N_i = 93,000 \text{ s}^{-1}$, while at the maxima of the interference pattern the signal count rate was about $N_s = 87,500 \text{ s}^{-1}$; at the minima it was about $N_s = 11,800 \text{ s}^{-1}$. The corresponding maximum and minimum rates of accidental coincidences were $N_{\text{acc}} = 32 \text{ s}^{-1}$ and $N_{\text{acc}} = 4 \text{ s}^{-1}$.

A glance at Fig. 3 suggests that the simple theory does a good job. To test it more closely, we fit the data with a parameterized version of Eq. (8)

$$N_c = N_0[1 + V \cos \delta], \quad (10)$$

where $\delta = (f_0 + f_1 v_p) v_p + \delta_0$, with the fitting parameters N_0 , V , f_0 , f_1 , and δ_0 . The quantity N_0 normalizes Eq. (8) to the data and the quantity V sets the depth of the minima. The inclusion of the linear and quadratic frequency terms, respectively f_0 and f_1 , in the fit takes into account the non-linear variation of the displacement of the piezo as a function of the applied voltage.

The quantity V is an important parameter often called the “visibility.” It is defined as

$$V = \frac{N_{\text{max}} - N_{\text{min}}}{N_{\text{max}} + N_{\text{min}}} = \frac{P_{\text{max}} - P_{\text{min}}}{P_{\text{max}} + P_{\text{min}}}, \quad (11)$$

where N_{max} and N_{min} are the maximum and minimum counts in the interference oscillation. As Eq. (11) indicates, the visibility can be defined equivalently in terms of the maximum and minimum probabilities P_{max} and P_{min} .

The visibility provides a measure of the completeness of the interference; $V = 1$ represents full interference when $\Delta\ell = 0$. When $\Delta\ell$ is increased, the visibility of the interference fringes decreases. As explained in the following, V be-

comes zero, that is, interference disappears when the experiment is capable of distinguishing which path a photon takes in passing through the apparatus. Our data give $V = 0.85 \pm 0.05$.¹⁶

Note the strength of the evidence that the interference is occurring one photon at a time. For one thing, it is very improbable that at any given instant there is more than one photon in the apparatus. If we take into consideration the effect of the optics, filters, and detector, we estimate the detection efficiency to be $\eta_{\text{det}} \sim 0.10$. With the length of the arms of the interferometer at $\ell \sim 21.5 \text{ cm}$, and for a maximum recorded counts of the signal singles ($N_s = 87500 \text{ s}^{-1}$), the average number of photons in the interferometer at any given time is never more than $\ell N_s / \eta_{\text{det}} c = 6 \times 10^{-4}$. Moreover, we record only those photons detected in coincidence with their down-conversion partner photon, an even smaller number. These results drive home to students that the interference pattern arises from the interference of each individual photon with itself.¹⁷

C. One-photon interference: Entanglement, distinguishability, and coherence

Although Feynman’s approach explains simply how the basic interference patterns arise, more complicated probability amplitudes are needed to explain partial interference and to give students some insight into the coincidence process. More complete probability amplitudes would include the effects of features of the apparatus such as filters, apertures, mirrors, beam splitters, and the distances between components, as well as the spectral purity, intensity, polarization, and angular spread of photon beams passing through the apparatus. These calculations, which can be complicated and difficult, usually result in one or more mathematical objects that have a spatial and temporal extent and which can be thought of as amplitude packets analogous to the wave packets of classical theory. Interference then arises from linear combinations of two or more overlapping packets.

As explained in the following, the basic features of an amplitude packet are ultimately determined by the Heisenberg uncertainty principle. We can sometimes use this principle to determine the spatial or temporal spread of a packet without doing detailed calculations. Such information makes it possible to tell when two amplitude packets will have appreciable values at the same place at the same time. Only then can there be interference. We can understand partial interference as occurring from the partial overlap of amplitude packets with well defined phases.

The overlap of amplitude packets also is related to the issue of distinguishability versus indistinguishability. When amplitude packets corresponding to different ways for an apparatus to give rise to the same observational outcome overlap in space and time, the apparatus does not distinguish between the different ways to the same outcome. When the packets do not overlap, the output from the apparatus contains information distinguishing between the alternatives. Although there are some pitfalls, in general, the nonoverlap of packets is equivalent to the distinguishability of alternatives, and in either case there will be no interference.

The down-conversion process itself produces amplitude packets with spatial spread. Although the pump-laser field has a very small spread of wave numbers and so can be well represented by plane-wave amplitudes, down-conversion photons emerge with a considerable spread of wave numbers

Δk . The uncertainty principle tells us that there will be a corresponding spatial spread of at least the order of $\Delta x = 1/\Delta k$. Thus a large spread in k means a narrow spread in x which in turn means that it will be technically difficult to overlap two such amplitude packets.

The spread of the amplitude packets of the down-conversion photons occurs even though conservation of energy assures that $k_i + k_s = k_p$ to within the very narrow energy spread of the pump laser. There can be appreciable variation in the individual values of k_i and k_s without violating the conservation of energy, because k_i is allowed to deviate from k_0 by some amount, call it $+k$, if k_s deviates by a compensating amount $-k$. Down conversion produces pairs with $k_i = k_0 + k$ and $k_s = k_0 - k$ with appreciable values for k , where k_0 is the central wave number (that is, $k_0 = k_p/2$). As a result, down-conversion photon pairs have a much wider spread of energy than the pump photons, and they also are strongly correlated in energy because whatever the sign and amount of k for the idler photon, the signal photon must have k of the same magnitude and opposite sign.

This energy correlation of the down-conversion photons is a manifestation of an unique quantum property called ‘‘entanglement.’’ Entanglement refers to the production of two (or more) particles in a state that has correlated properties (such as $k_0 + k$ and $k_0 - k$), but where neither particle possesses a definite property until a measurement is made. In our case entanglement means that neither down-conversion photon is in the state $k_0 + k$ until a measurement is made. The measurement of one photon puts it randomly into a definite state and the other photon goes automatically into the correlated state. Thus if a measurement of the idler photon yields $k_0 - k$, the signal photon will then be in the state $k_0 + k$, and vice versa. An example of a state vector representing such entanglement before the measurement is

$$|\psi\rangle = \frac{1}{\sqrt{2}} (|k_0 + k\rangle_s |k_0 - k\rangle_i + |k_0 - k\rangle_s |k_0 + k\rangle_i), \quad (12)$$

where the subscripts s and i refer to the signal and idler photons. Although Eq. (12) is a special case, it illustrates the characteristic property of an entangled state: It is a nonfactorable combination of single-particle states.

A very general representation of the possible states of a pair of down-conversion photons is the continuous superposition of state vectors^{5,18,19}

$$|\psi_{s,i}\rangle = \int dk_s \int dk_i \phi(k_s, k_i) |k_s\rangle_s |k_i\rangle_i \delta(k_s + k_i - k_0), \quad (13)$$

where $\delta(k_s + k_i - k_0)$ is the Dirac delta function. The details of this general state reside in the form of the amplitude $\phi(k_s, k_i)$, which can be and usually is a function of many more variables than k . If $\phi(k_s, k_i)$ is not factorable into separate functions of k_s and k_i , the state is entangled. As we have noted, the apparatus can shape $\phi(k_s, k_i)$ to be nonzero over a restricted range of Δk around k_0 and result in an amplitude packet arising from a coherent superposition of correlated energy eigenstates with some range of energies $\Delta E = c\hbar\Delta k$ and with a corresponding spatial extent.

In our experiments the bandwidth of a packet reaching our detectors is determined chiefly by irises that define the paths

of the beams and by bandpass filters in front of the detectors. By knowing the properties of these components, we can estimate the size of an amplitude packet, relate it to the coherence length, and use it to explain when an interference pattern will occur and when it will fade away.

We already mentioned that an equivalent analysis is possible in terms of distinguishability and indistinguishability. Although indistinguishability is a somewhat slippery concept, it is reasonably clear how to apply it to our interference experiments. By measuring the time delay between the idler and signal photons, our apparatus can, in principle, distinguish a longer path taken by a photon passing through the interferometer from a shorter path. The time delay between the detection of the tag photon and the photon passing through the interferometer will be longer when the photon takes the longer interferometer path than when it takes the shorter one. The time delay will be the difference in path lengths $\Delta\ell$ divided by c , the speed of light.

The spread Δk of the wave numbers of the down-conversion photons leads to a spread Δt in the difference between the times when the two photons arrive at their detectors. As long as the difference in path lengths through the two interferometer arms does not correspond to a difference of travel time greater than Δt , we cannot distinguish which path the signal photon took through the interferometer. But when the difference in interferometer path lengths $\Delta\ell$ becomes large enough so that $\Delta\ell/c > \Delta t$, the time at which a photon taking the longer path is detected in coincidence with the idler will be distinguishably longer than that of a photon taking the shorter path. In principle, we will then be able to distinguish which path a photon takes, and there should be no interference. The distance $c\Delta t$ is a measure of the spatial extent of the amplitude packet and is called its coherence length ℓ_c . Thus we expect that with $\Delta\ell \approx 0$, there should be an interference pattern, but when $\Delta\ell$ becomes the order of ℓ_c , the amplitude packets no longer fully overlap at the interferometer output and the pattern fades away.

D. One-photon interference with different coherence lengths

We control the value of ℓ_c in our experiments by limiting the spread of wave numbers Δk with bandpass filters placed in front of the detectors. The properties of such filters are usually expressed in terms of the spread of wavelengths $\Delta\lambda$ that they transmit around a central wavelength λ_0 . Hence, it is customary to express $\ell_c = c\Delta t$ in terms of these quantities. Because $k_0 = 2\pi/\lambda_0$, it follows that $\Delta k = 2\pi\Delta\lambda/\lambda_0^2$ if $\Delta\lambda$ is small compared to λ_0 . Then the coherence length $\ell_c = \lambda_0^2/\Delta\lambda$. The data shown in Fig. 3 were taken with $\lambda = 915.8$ nm down-conversion photons and with 10 nm bandpass filters in front of the detectors. The corresponding coherence length is 84 μm .

As $\Delta\ell$ increased and approached ℓ_c , the visibility of the data in Fig. 3(a) decreased. For example, when we increased $\Delta\ell$ to 36 μm by turning the micrometer of the linear stage where the piezo-driven mirror was mounted, we measured fringes (not shown) with a lower visibility $V = 0.31 \pm 0.05$. When $\Delta\ell$ was increased to 144 μm , we obtained the data shown by the circles in Fig. 3(b). In other words, when the path lengths through the interferometer differed by more than ℓ_c , the fringes disappeared into the noise. When the differ-

ence in path length through the interferometer arms is this large, the packets do not overlap, and the apparatus is capable of distinguishing which path a given photon took. The amplitudes then combine according to Feynman's rule 3, and there is no interference, that is, $P = 2RT$.

As a dramatic demonstration of the effect of the magnitude of the coherence length, we placed a 0.1 nm filter in front of the idler detector with $\Delta\ell = 144 \mu\text{m}$. The new filter increased the coherence length to $8400 \mu\text{m}$, and, as can be seen by the squares in Fig. 3(b), the fringes reappeared with a visibility of $V = 0.59 \pm 0.04$.

Note that we placed the 0.1 nm filter in front of the idler detector and *not* in front of the signal detector. Because of the entanglement between the idler and the signal photons, it makes no difference whether we change the filter in front of the idler detector or the one in front of the signal detector. The signal detector had a 10 nm filter in front of it. This result is a dramatic demonstration of the energy correlation between the two photons. Reference 20 gives an interesting interpretation of this result in terms of the collapse of the wavefunction of the idler and signal photons.

IV. BIPHOTON INTERFERENCE

In the one-photon experiment, interference arose from the superposition of the two amplitudes describing two indistinguishable alternate paths by which a single photon could produce the same outcome. If we send two collinear photons into the interferometer, the number of alternatives increases to four, and the outputs are determined by the superposition of four amplitudes. We should expect that the interference pattern arising from four amplitudes will be more complicated than the one observed in the one-photon experiment, as is indeed the case. Two-photon experiments exhibit interference that is fourth-order in the electric field rather than second-order as in the more familiar single-photon interference experiments described in Sec. III A.^{18,19}

A. Biphoton: Experimental results

We did two-photon experiments with a Michelson interferometer used as described in Refs. 21 and 22. As shown in Fig. 1(b), photons from the 402.4 nm pump laser entered a down-converter crystal oriented to emit a collinear pair of equal-wavelength photons. The crystal sat between two crossed polarizers. The first polarizer ensured that pump photons entered the crystal horizontally polarized, and the second polarizer ensured that only vertically polarized down-conversion photons entered the interferometer. The entangled pair of down-conversion photons passed through the Michelson interferometer and then to a beam splitter, each output of which was viewed by an avalanche photodiode detector. We recorded only the events that produced coincidences between the two detectors.

Our data are shown in Fig. 4. They are coincidences plotted as a function of δ , which was extracted from the fits to the data, as described earlier. The data were taken with three different interferometer settings: $\Delta\ell \sim 0$ (squares), as verified with white-light fringes, $\Delta\ell \sim 47 \mu\text{m}$ (circles), and $\Delta\ell \sim 210 \mu\text{m}$ (triangles). Both detectors had 10 nm filters in front of them. As is particularly apparent in the data of solid circles, the resulting interference patterns are the sum of two oscillations, one with a frequency twice that of the other.

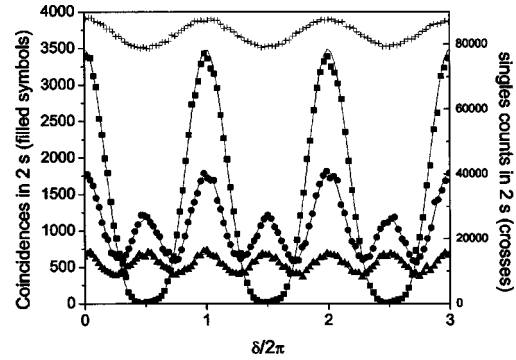


Fig. 4. Data for the interference of two collinear photons going through the Michelson interferometer. The coincidence data correspond to the cases when the path-length difference $\Delta\ell$ was approximately 0 (squares), $47 \mu\text{m}$ (circles), and $210 \mu\text{m}$ (triangles). The crosses (+) are the data collected by a single detector when $\Delta\ell = 37 \mu\text{m}$.

There are two interference patterns present, and the data show a progression in which one pattern remains and the other fades away as $\Delta\ell$ is increased.²³

B. Biphoton: Interpreting the results

The pattern for $\Delta\ell \sim 0$ can be predicted by the same method that we used to predict the one-photon interference pattern. We identify the possible paths through the interferometer and write down the corresponding plane-wave amplitudes modified by appropriate factors of r and t as they pass through the interferometer. Because there are two photons, each path will have associated with it the product of two single-photon amplitudes. The wave numbers in these factors must be modified to take entanglement into account.

For example, consider the possibility corresponding to case A of Fig. 5. Here the two entangled photons are viewed as traveling together in arm 1. With r and t being respectively the reflection and transmission amplitudes of the interferometer's input beam splitter, the amplitude is $rte^{i(k_0+k)\ell_1}rt e^{i(k_0-k)\ell_1} = r^2t^2e^{i2k_0\ell_1}$. The use of $+k$ in one

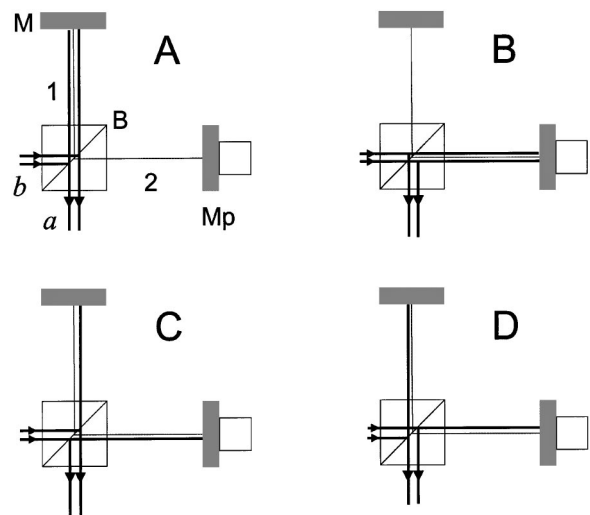


Fig. 5. Four possible paths for two collinear photons in a Michelson interferometer. The labeled components are nonpolarizing 50-50 beam splitter (B), mirror (M), and mirror moved by a piezoelectric stack (Mp). The output ports are labeled a and b .

factor and $-k$ in the other takes into account entanglement by specifying that if one photon differs from the central wave number k_0 by $+k$, the other must differ by $-k$. For this particular amplitude the two deviations from the central wave number cancel.

For the path corresponding to two photons traveling through arm 2, a similar argument gives $t^2 r^2 e^{i2k_0 \ell_2}$. Note that the presence of two photons in the same arm of the interferometer multiplies the phase of the amplitude by a factor of 2.

We also must include the amplitudes for cases C and D of Fig. 5. In case C, one photon, say the idler, is imagined as traveling through arm 1 while the signal photon travels through arm 2. The corresponding amplitude is $r t e^{i(k_0+k)\ell_1} t r e^{i(k_0-k)\ell_2}$. There is a similar amplitude for the same paths but with the two photons interchanged. In these amplitudes there is no cancellation of the wave vector deviations k .

The probability of passing through the interferometer is the square of the modulus of the sum of the probability amplitudes for cases A, B, C, and D,

$$P_2 = |r^2 t^2 (e^{i2k_0 \ell_1} + e^{i2k_0 \ell_2} + 2 \cos[k(\ell_1 - \ell_2)] e^{ik_0(\ell_1 + \ell_2)})|^2 \quad (14a)$$

$$= 2R^2 T^2 (1 + 2 \cos^2[k\Delta\ell] + 4 \cos[k\Delta\ell] \cos \delta + \cos 2\delta). \quad (14b)$$

Notice that if $k\Delta\ell \ll 1$ Eq. (14) simplifies to

$$P_2 = 2R^2 T^2 [3 + \cos 2\delta + 4 \cos \delta] \quad (15a)$$

$$= 4R^2 T^2 [1 + 2 \cos \delta + \cos^2 \delta] \quad (15b)$$

$$= 4R^2 T^2 [1 + \cos \delta]^2. \quad (15c)$$

The result of Eq. (15c) predicts fringes that are narrower than the single-photon interference fringes. In this respect these quantum multiple-path interferences are analogous to multiple-beam wave interference: the more interfering paths (or beams), the narrower the fringes.²⁴ The curve passing through the squares in Fig. 4 shows that Eq. (15c) provides an excellent fit to our data for the case when $\Delta\ell \approx 0$.

We can arrive at the same theoretical interpretation using the state vector formalism. We start with a symmetrized wavefunction like Eq. (12), and replace the input wavefunctions by coherent superpositions of the wavefunctions for going through each arm, as done in Sec. III A for the case of the single photon. The photon leaving the interferometer away from the source is in state $|a\rangle$, and the photon returning to the source is in state $|b\rangle$. The state vectors then become

$$|k_0 \pm k\rangle_{s,i} = r e^{i(k_0 \pm k)\ell_1} (t|a\rangle_{s,i} + r|b\rangle_{s,i}) + t e^{i(k_0 \pm k)\ell_2} (r|a\rangle_{s,i} + t|b\rangle_{s,i}). \quad (16)$$

After some algebra we find that the state vector is given by

$$|\psi\rangle = \alpha|a\rangle_s|a\rangle_i + \beta|a\rangle_s|b\rangle_i + \gamma|b\rangle_s|a\rangle_i + \epsilon|b\rangle_s|b\rangle_i, \quad (17)$$

where α , β , γ , and ϵ are complex functions of the interferometer lengths and wavenumbers. Because we detect the case when both photons leave the interferometer in state $|a\rangle$, the probability that both photons go through the interferometer is

$$P_2 = |\langle a|_s \langle a|_i |\psi\rangle|^2 = \alpha^* \alpha, \quad (18)$$

where

$$\alpha = \sqrt{2} r^2 t^2 [e^{i2k_0 \ell_1} + e^{i2k_0 \ell_2} + 2 e^{ik_0(\ell_1 + \ell_2) \cos k(\ell_1 - \ell_2)}]. \quad (19)$$

We substitute Eq. (19) into Eq. (18) to obtain Eqs. (14a) and (14b).²⁵

In our setup cases C and D can become distinguishable while A and B remain indistinguishable. This case occurs when we increase $\Delta\ell$ to about 210 μm . Then we obtain the data represented by the triangles in Fig. 4. If we apply Feynman's rule to a situation where cases C and D are distinguishable, we must add their contributions separately to the final probability. Cases A and B remain indistinguishable, so

$$P_2 = |r^2 t^2 (e^{i2k_0 \ell_1} + e^{i2k_0 \ell_2})|^2 + R^2 T^2 + R^2 T^2 \quad (20a)$$

$$= 2R^2 T^2 [1 + \cos 2\delta] + 2R^2 T^2 \quad (20b)$$

$$= 4R^2 T^2 \left[1 + \frac{1}{2} \cos 2\delta \right]. \quad (20c)$$

Equation (20c) predicts both the reduction in the magnitude of the amplitude and the doubling of the fringe frequency shown by the triangles in Fig. 4. For comparison note that the single-photon fringes (the crosses in Fig. 4) obtained by one of the detectors when $\Delta\ell \sim 37 \mu\text{m}$ clearly have a frequency which is half that of the two-photon fringes.

We fit our data with a version of Eq. (14b) parameterized to describe the visibilities of different parts of the overall pattern:

$$N_c = N_0 [2 + V_0 + 4V_{CD} \cos \delta + V_{AB} \cos 2\delta], \quad (21)$$

where N_c is the number of counts recorded in some chosen time interval. V_0 and V_{CD} are related to the visibility of the one-photon pattern, and $V_{AB}/2$ is the visibility of the two-photon interference pattern. We will give further justification for this parameterization in the following section.

The data recorded when the difference in path lengths through the interferometer is zero (squares in Fig. 4) are well fit by the solid line which is Eq. (21) with $N_0 = 442 \pm 13$ counts/(2s), $V_{AB} = 0.98 \pm 0.08$, and $V_{CD} = 0.98 \pm 0.02$ ($V_0 = 0.99 \pm 0.02$). That is, the data are consistent with Eq. (15); there is full indistinguishability of the four possibilities. When the path lengths through the arms were made to differ by 47 μm , we obtained the data represented by the circles; these are well fit using $V_{AB} = 0.81 \pm 0.09$ and $V_{CD} = 0.15 \pm 0.07$. These visibilities show that cases C and D are becoming distinguishable while A and B remain indistinguishable. Finally, when the path-length difference was increased to 210 μm , the part of the pattern arising from the possibilities of the photons taking separate paths (that is, cases C and D) essentially vanishes, and the data (triangles in Fig. 4) are fit using just $V_{AB} = 0.51 \pm 0.13$ and $V_{CD} = 0.01 \pm 0.05$. This result is consistent with Eq. (20c).

C. Biphoton: Calculating the coherence length

To understand why the above data behave as observed, we need probability amplitudes that take into account the finite spread in wave numbers. We avoid the complete theory,²⁶ but construct model amplitudes complicated enough to contain the essential features of the experiment and simple enough to allow students to work quantitatively with the concepts of coherence length and entanglement. We make such model amplitudes by assuming that the values of k that appear in

Eq. (14b) are distributed uniformly over an interval Δk centered on k_0 . We then build the amplitudes by integrating the relevant terms.

We replace $2 \cos^2(k\Delta\ell)$ in Eq. (14b) by $(1 + \cos 2k\Delta\ell)$ and integrate over the uniform distribution of k to find

$$P_2 = 2R^2T^2 \left(1 + \frac{1}{\Delta k} \int_{-\Delta k/2}^{+\Delta k/2} (1 + \cos 2k\Delta\ell) dk \right. \\ \left. + 4 \left\{ \frac{1}{\Delta k} \int_{-\Delta k/2}^{+\Delta k/2} \cos(k\Delta\ell) dk \right\} \cos \delta + \cos 2\delta \right). \quad (22)$$

The first integral in Eq. (22) gives $[1 + \text{sinc}(\Delta k\Delta\ell)]$, and the second gives $\text{sinc}(\Delta k\Delta\ell/2)$, where the sinc function is defined as,

$$\text{sinc}(x) \equiv \frac{\sin x}{x}, \quad (23)$$

and might be familiar to students who have analyzed single-slit diffraction. For $x=0$, $\text{sinc}(0)=1$, and as x increases, $\text{sinc}(x)$ oscillates with diminishing amplitude around the x axis. Its first zero occurs when $x=\pi$, that is, $\text{sinc}(\pi)=0$.

The result is that with a uniform distribution of wave numbers, Eq. (14b) predicts that

$$P_2 = 2R^2T^2 (2 + \text{sinc}[\Delta k\Delta\ell] + 4\text{sinc}[\Delta k\Delta\ell/2] \\ \times \cos \delta + \cos 2\delta). \quad (24)$$

The sinc terms result in the loss of interference when the distance a photon travels in one arm of the interferometer becomes appreciably different from the distance it travels in the other. Both sinc functions go to zero when $\Delta\ell$ becomes appreciably larger than $1/\Delta k$. The smallest value of the argument for which both become identically zero is $\Delta k\Delta\ell = 2\pi$. This value occurs when $\Delta\ell = 2\pi/\Delta k$, the quantity earlier identified as the coherence length ℓ_c .

When either $\Delta k=0$ as for our earlier plane wave treatment or when $\Delta\ell \approx 0$ (white-light fringes), Eq. (24) reduces to Eq. (15a). And when the difference in the lengths of the paths that they travel through the interferometer arms becomes large relative to the coherence length, the terms in Eq. (24) multiplied by the sinc functions drop out, and Eq. (24) reduces to Eq. (20c).

This analysis confirms our earlier interpretation. The interference patterns of Fig. 4 arise from two different modes of interference. In the AB mode the biphoton produces the interference pattern of a single photon with the wave number and the longer coherence length of the pump laser—so long that we did not include it in our analysis. The CD mode of the biphoton produces single-photon interference of down-conversion photons with the much shorter coherence length that they acquire in down conversion. The presence of the two modes and the fading of the CD mode as $\Delta\ell$ is increased to and beyond the CD coherence length explain the progression of the curves in Fig. 4.

Our biphoton experiments are a reminder to be careful interpreting Dirac's statement that "interference between two different photons never occurs."¹⁷ As Glauber has pointed out,²⁷ it is amplitudes that interfere. The biphoton illustrates that interference can occur regardless of the number of photons involved.

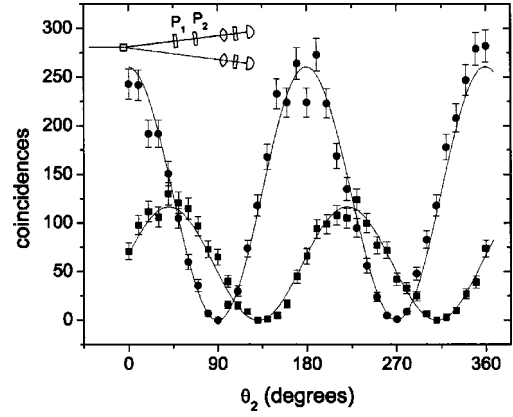


Fig. 6. Coincidences per second as a function of the orientation of polarizer P_2 in front of the signal detector for two settings of polarizer P_1 located as shown schematically in the insert.

V. POLARIZATION AND INTERFERENCE

A. Polarizer as a wavefunction projector

We can use a polarizer to transform the polarization states of our photons. The effect of the polarizer is conveniently described in terms of vectors corresponding to its transmission and extinction directions. If we represent the horizontally and vertically polarized states of photons as $|H\rangle$ and $|V\rangle$, respectively, the polarizer with its transmission axis forming an angle θ with the horizontal will transform the photon states into the new basis states

$$|T_\theta\rangle = \cos \theta |H\rangle + \sin \theta |V\rangle \quad (25)$$

for the transmission axis, and

$$|E_\theta\rangle = -\sin \theta |H\rangle + \cos \theta |V\rangle \quad (26)$$

for the extinction axis. Because the polarizer transmits photons in the $|T_\theta\rangle$ state and absorbs photons in the $|E_\theta\rangle$ state, the transmission probability of a photon in state $|\psi\rangle$ is

$$P = |\langle T_\theta | \psi \rangle|^2. \quad (27)$$

As we have noted, the type-I down conversion of our experiments generates two vertically polarized photons, that is, in the state $|V\rangle$. In an experiment where the down-conversion beams went directly to the detectors, we placed two polarizers, labeled 1 and 2, on the path of the signal beam as shown in the insert to Fig. 6. We set polarizer 1 with its transmission axis vertical (that is, $\theta_1 = \pi/2$), and varied the angle θ_2 of the second polarizer. The circles in Fig. 6(a) show that the variation of the coincidences as a function of θ_2 is well described by

$$P = |\langle T_{\theta_2} | V \rangle|^2 = \sin^2 \theta_2. \quad (28)$$

But the polarizer does much more: it also projects the photon state onto the transmission state. That is, the state of the photon after the polarizer is $|T_\theta\rangle\langle T_\theta | \psi \rangle$. If we rotate polarizer 1 so that it forms an angle θ_1 with the horizontal, then the state of the photon before the second polarizer will be $|T_{\theta_1}\rangle\langle T_{\theta_1} | \psi \rangle$, and the transmission probability will be

$$P = |\langle T_{\theta_2} | T_{\theta_1} \rangle \langle T_{\theta_1} | \psi \rangle|^2 = \cos^2(\theta_2 - \theta_1) \sin^2 \theta_1. \quad (29)$$

The squares in Fig. 6 represent the data for $\theta_1 = 3\pi/4$, and are consistent with

$$P = \frac{1}{2} \cos^2(\theta_2 - 3\pi/4). \quad (30)$$

The lines in Fig. 6 are fits of the function $N_c = N_0 \cos^2(\theta_2 - \phi)$ to the two data sets. The amplitudes N_0 of the fits have a ratio of 0.45 ± 0.10 , and the fitted phases ϕ differ by $41^\circ \pm 3^\circ$, consistent with our expectations. Notice that the minima of the two graphs in Fig. 6 do not occur at the same angles. When $\theta_1 \neq \pi/2, 3\pi/2$, the probability is no longer zero at $\theta_2 = n\pi$ (integer n).

B. The quantum eraser

Our quantum eraser experiment, which is like those of Ref. 28, further illustrates the importance of indistinguishability and which-way information. (Schneider and LaPuma²⁹ have recently reported using an attenuated source to do a similar experiment.)

We arranged our apparatus as described in Sec. III A, but with a first-order quartz half-wave plate in one arm of the interferometer and a dummy quartz wave plate in the other arm to compensate for the added optical path length (dashed rectangles in Fig. 1). By aligning either axis of the half-wave plate (fast or slow) with the polarization of the down-conversion light (that is, vertical) and stepping the voltage v_p on the piezo, we obtained the graph shown by the squares in Fig. 7. The result is well described by a parameterized version of Eq. (8). A least-squares fit to $N_0(1 + V \cos \delta)$ gave $N_0 = 392 \pm 20$ (counts per 20 s) and $V = 0.79 \pm 0.06$.

The rotation of the half-wave plate by an angle ϕ rotates the polarization by 2ϕ . The state of the photon emerging from arm 1 is given by

$$|\ell_1\rangle = rt[\cos 2\phi|V\rangle + \sin 2\phi|H\rangle], \quad (31)$$

and the probability of detecting it is

$$P = RT|e^{i\delta_1}|\ell_1\rangle + e^{i\delta_2}|V\rangle|^2 = \frac{1}{2}(1 + \cos 2\phi \cos \delta), \quad (32)$$

for $R = T = 1/2$. When $\phi = \pi/4$, there is no interference (that is, $P = 1/2$) because the apparatus associates a distinct polarization state with each possible path: $|V\rangle$ for one path and $|H\rangle$ for the other. This setting of the wave plate has the effect of making the paths distinguishable, and the presence of such distinguishing information results in the absence of interference even if the photon's polarization state is not measured. The circles in Fig. 7 show the data obtained when $\phi = \pi/4$. A fit gives $N_0 = 286 \pm 18$ (20 s)⁻¹ and $V = 0.01 \pm 0.08$, showing that there is indeed no interference.

We can erase the distinguishing information by projecting the two orthogonal states with a polarizer set to $\pi/4$ relative to the horizontal and located *after* the interferometer. The projection amplitudes between $|H\rangle$ and $|V\rangle$ and the polarizer state $|T_{\pi/4}\rangle$ are the same. The state of each photon after such a polarizer is

$$|T_{\pi/4}\rangle (\langle T_{\pi/4}|H\rangle e^{i\delta_1} + \langle T_{\pi/4}|V\rangle e^{i\delta_2}), \quad (33)$$

so the probability of detecting a photon is

$$P = \frac{1}{2}(1 + \cos \delta). \quad (34)$$

The triangles in Fig. 7 show the data obtained with a polarizer oriented at $\theta = \pi/4$ after the interferometer. A fit to the data gives $N_0 = 64 \pm 8$ (20 s)⁻¹ and $V = 0.82 \pm 0.12$, showing that the polarizer erased the distinguishing information. The inserted polarizer inherently attenuated the light by 0.46

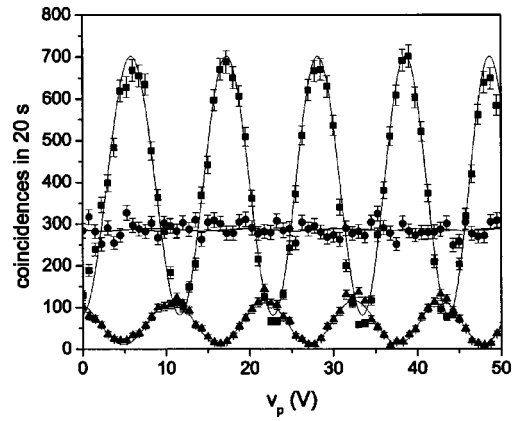


Fig. 7. Data from the quantum eraser experiment when the interferometer paths are indistinguishable (squares), distinguishable (circles), and when the distinguishing information is erased by placing a polarizer after the interferometer (triangles).

± 0.01 at these wavelengths. If we correct for this attenuation, the ratio of the two amplitudes is 0.47 ± 0.10 , consistent with the predicted $1/2$.

We have introduced this experiment (with $\phi = \pi/4$) in our first-year introductory physics class. The experiment illustrates some of the basic ideas of quantum mechanics discussed in this course.³⁰ Because there was only one setup, students took turns doing the experiments. The results were explained using the concepts of the distinguishability of paths.

VI. DOES THE PHOTON EXIST?

Is there actually such a thing as a photon? We wanted students to confront this question, because it is fundamental to the interpretation of our experiments and because the evidence for the photon is less obvious than students are given to think. The Compton effect and the photoelectric effect are usually cited as evidence for the photon's existence, but both effects can be explained as arising from the interaction of a continuous (classical) electromagnetic field with matter possessing quantized energy states. Such "semiclassical" theories have no photons; quantum properties are associated only with matter, not with the electromagnetic field.

Tagging the signal photon with the idler photon allows us to say with considerable certainty that the amount of energy in our apparatus corresponds to the energy of a single photon. Consequently, if we direct this energy onto a 50-50 beam splitter and look with detectors at the two outputs, we should be able to distinguish experimentally between the semiclassical theory with its continuous field and the fully quantum theory with its discrete photons.

In the semiclassical case the two detectors should register counts in coincidence with each other. The semiclassical explanation of the photoelectric effect³¹ predicts that detectors using the photoelectric effect and sensitive to some frequency f —the kind of detector used in most quantum optics experiments, including ours—can register counts when illuminated with light down to arbitrarily low intensity levels. If there were no such thing as a photon, an electromagnetic wave striking a 50-50 beam splitter would divide if the semiclassical wave picture is applicable. Half of its energy would

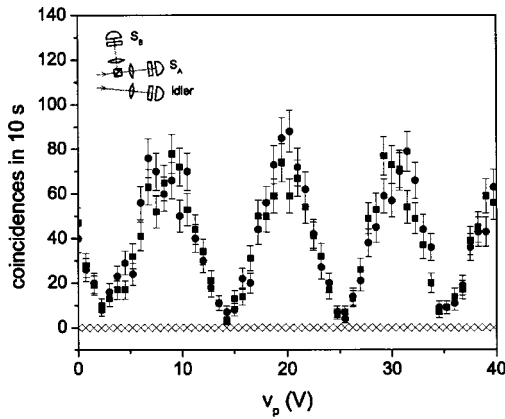


Fig. 8. Interference data for signal photons that go through a Mach–Zehnder interferometer and reach a beam splitter with two detectors S_A and S_B located at its output ports as shown in the insert. The circles and squares correspond to double coincidences of the idler detector with S_A and S_B , respectively. Symbols (\times) correspond to triple coincidences of the idler detector, S_A , and S_B .

emerge from one output and half from the other, and the detector at one output should detect electromagnetic energy in coincidence with the detector at the other.

If the field is quantized, however, there should be no coincidences. If the field quantum, the photon, exists and is indivisible, and if there is only one in the system, the detection of a photon at one output means no photon will be detected at the other. In the absence of background radiation, we should never detect electromagnetic radiation at one detector in coincidence with the other.

With our apparatus we could have performed a version of the 1986 experiment by Grangier, Roger, and Aspect,³² which shows conclusively that photons never divide at a beam splitter. Greenstein and Zajonc³¹ have given a particularly clear and well written analysis of the results of Ref. 32. Recently, Beck and colleagues have used down-conversion to do a similar experiment in an undergraduate setting.³³

We did not test photon behavior at a beam splitter as thoroughly as in Refs. 32 or 33. Instead, we did an experiment that could be set up quickly from the existing configuration for the interference measurements and give results in a few minutes of data taking. Our approach was to add a third beam splitter at the output of the interferometer, with a lens-filter-detector set located at each of its output ports, as shown in the insert in Fig. 8. The signal photons could then either transmit to detector S_A , reflect to detector S_B , or potentially split and be detected by both. For every signal photon passing through the beam splitter (that is, via transmission or reflection), the probability of detecting it is $P_A = P_B = \eta_{\text{pbs}}$, where η_{pbs} is the detection efficiency past the beam splitter. For our apparatus we estimated $\eta_{\text{pbs}}(\lambda = 915.8 \text{ nm}) = 0.18 \pm 0.02$, the product of the transmission efficiency through the lens and filter (0.51 ± 0.02) and the quantum efficiency of the detector (0.36 ± 0.02).⁶ The probability for two simultaneous detections at detectors A and B is $P_{AB} = \eta_{\text{pbs}}^2 = \eta_{\text{pbs}} P_A = \eta_{\text{pbs}} P_B$. Thus, if every photon that contributes to the interference pattern splits at the third beam splitter, the triple coincidences between the idler, S_A and S_B should be about 18% of the coincidences between the idler and S_A or S_B .

We used a second TAC/SCA and another coincidence cir-

cuit to detect double coincidences of the idler detector with S_A and the idler detector with S_B ; triple coincidences were recorded as coincidences of the doubles. The idler detector had a 1 nm filter in front of it, and the two signal detectors had 10 nm filters in front of them.

The time window for coincidences in the doubles was set to 40 ns. Each double coincidence was recorded when the signal photon (A or B) arrived within 10 ns of the idler photon. The predicted rate of accidental coincidence of doubles for our setup was $< 2 \times 10^{-6} \text{ s}^{-1}$. We tested our coincidence electronics with fake triple coincidence pulses generated by a digital-delay pulse generator.

Figure 8 shows three sets of data. The coincidences between the idler detector and signal detector S_A (squares), and the coincidences between the idler detector and signal detector S_B (circles) show interference fringes as the path length difference of the interferometer is varied via the piezo voltage v_p . The triple coincidences (\times in Fig. 8) do not show any counts. As we noted, had each of the photons split at the third beam splitter, we would expect an interference pattern in the triple coincidences with an amplitude of about 12 counts in 10 s. Consequently, our data are consistent with the conclusion that some appreciable number of the photons do not split.

VII. SUMMARY AND CONCLUSIONS

We have developed undergraduate level experiments that use a source of correlated pairs of photons to illustrate basic principles of quantum mechanics. The results from our tabletop experiments are simply explained when the interferometers are adjusted to have nearly equal length arms. In this case we can use Feynman's explanation of quantum interference in terms of simple plane-wave probability amplitudes. With the help of the concept of coherence length, more complicated situations of interference can be understood in terms of distinguishability and indistinguishability. The interference of single photons also provides a physical situation in which students can learn to use state vectors to investigate state projection, basis change, and the calculation of probabilities for a particular outcome. The experiments also provide dramatic teaching moments for the discussion of fundamental questions about the nature of light and the concepts of quantum mechanics.

The experimental setup fits on a $2' \times 4'$ optical breadboard, requiring laboratory components that individually do not exceed \$7000. The experiments can be done without previous research experience with photon quantum optics.

The single-photon experiments presented here can be used in undergraduate courses in quantum mechanics for which laboratories and demonstrations are rare. By replacing the down conversion crystal, the apparatus can be used to measure the violation of Bell's inequalities.² The building phase of each experiment makes an excellent upper level undergraduate project.

ACKNOWLEDGMENTS

We are indebted to P. Kwiat, whose ideas and help were invaluable to the success of this project. We also thank A. Zeilinger and T. Jennewein for their assistance, M. Beck, J. Eberly, S. Malin, M. E. Parks, and W. Wooters for helpful discussions, and S. J. Hinterlong and R. Williams for help

Table I. Prices of essential components of the basic setup.

Description	Vendor	Model	Each	No.	Comment
Diode laser	Power Technology	1Q2C18/5911	\$6400	1	$\lambda = 402.3$ nm, 18 mW
Crystal	Cleveland Crystals		\$1000	1	beta-barium-borate, $7 \times 7 \times 5$ mm
Crystal mounting	Thorlabs	PR01+KMPM	\$370	1	prism mount and rotation stage
Detectors	EG&G/Pacer	SPCM-AQR-13	\$4100	2	avalanche photodiode
Filters	Andover	CW/L	\$600	2	10 nm filter for $2\lambda_p$
Lens mount	Thorlabs	LM1XY	\$140	2	XY translation
TAC/SCA	Canberra	2145	\$1840	1	module
Multichannel scaler	Canberra	ASA-100	\$3500	1	computer card
Counter	National Instruments	PCI6601+BNC2121	\$700	1	4 counter PC card
Optical breadboard	Thorlabs	T2448A	\$1150	1	$2' \times 4'$

with the equipment. This work was funded by a grant from the National Science Foundation DUE-9952626.

APPENDIX A: COST OF COMPONENTS

We did not have prior experience with these types of experiments, and the cost of the essential components listed in Table I is intended for those with similar inexperience. The total cost of this essential equipment is about \$25,000. Table I does not include the standard mounting hardware or the optical hardware to steer the laser onto the down-conversion crystal, which may add about \$1,000 to the total price. The price of the blue diode laser that we list is for a module that includes current and temperature control and beam-shaping optics. The price of the bare laser diode is much lower (\$1000–2000).²

The essential equipment items for the experiments that we discussed are listed in Table II. The total cost of these elements is about \$6000. It does not include the mounting hardware and apparatus for steering the down-conversion beams in and out of the interferometer (4 mirrors plus mounting hardware). If we include all of them, the cost is about \$9000. A picture of the apparatus is shown in Fig. 9. As stated, the estimated cost is for “plug and play” parts, provided all is put together carefully. The cost can be lowered by customizing the electronics and hardware parts. We also tried several hardware arrangements. Most experiments were done with optics mounted in convenient magnetic mounts, linked by rods in the interferometers. We found “pedestal” mounting

hardware, where the optics are very close to the optical table, to be less versatile but simpler, less expensive, and more stable against vibrations.

APPENDIX B: DOWN CONVERSION

Spontaneous parametric down conversion is a well studied nonlinear optics effect. In brief, it involves the use of a birefringent crystal to convert an incident pump photon into two photons, the signal and the idler. As mentioned, this process conserves energy $E = \hbar ck$, so that

$$k_p = k_s + k_i, \quad (\text{B1})$$

where k_p , k_s , and k_i are the wave numbers in vacuum. Here we treat only degenerate down conversion where $k_s = k_i = k_p/2$. Consider the case where the down-conversion photons leave the crystal in different directions as shown in Fig. 1(a). If θ_c is the angle that the signal and idler photons form with the direction of propagation of the pump beam inside the crystal, then Eq. (3) becomes

$$n_p k_p = 2n_s k_s \cos \theta_c. \quad (\text{B2})$$

We combine $k_s = k_p/2$ with Eq. (B2) and obtain

$$n_p = n_s \cos \theta_c. \quad (\text{B3})$$

It is not possible to satisfy Eq. (B3) in an isotropic medium, because for normal dispersion the index of refraction decreases with increasing wavelength, that is, $n_p > n_s$. This problem can be overcome with a birefringent crystal. The top

Table II. Prices of essential components of the experiments.

Description	Vendor	Model	Each	No.	Comment
Cube beam splitter	Melles Griot	03BSC027	\$120	2	near-IR, nonpolarizing
Prism mount	New Focus	9411	\$310	2	Beam-splitter mount
Mirror mount	Thorlabs	KS1	\$80	2	high-stability mounts
Piezo stack	Thorlabs	AE0505D8	\$130	1	for changing $\Delta \ell$
Linear stage	Thorlabs	MT1	\$250	1	piezo mount goes on top
Filter	Andover	CW/L	\$850	1	1 nm filter for $2\lambda_p$
Wave plate	Melles Griot	02WRQ0023	\$690	1	half wave
Wave plate	Melles Griot	02WRQ0003	\$590	1	quarter wave
Polarizer	Edmund	A46088	\$250	2	Near-IR polarizer
Voltage amplifier	Trek	P0516A-1	\$700	1	0–150 V to drive piezo
PC interface	National Instruments	PCI6703+BNC2121	\$1400	1	PC card, connector box and Labview software

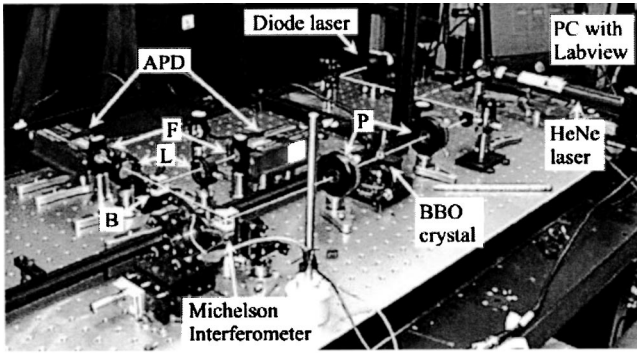


Fig. 9. Photograph of the layout for the biphoton experiments. The hardware is mounted on pedestal mounts, and the entire layout fits on a 2' x 4' optical breadboard. The path of the light beams is traced in white.

solid line in Fig. 10 represents the ordinary index of refraction, where the polarization of the light is perpendicular to the optic axis (OA) of the crystal. If the polarization is in the same plane as OA, the index of refraction, also known as the extraordinary index of refraction, depends on the angle θ_m formed between the propagation direction \mathbf{k}_p and OA. The lower solid line in Fig. 10 corresponds to the case where $n_e = \tilde{n}_e(\theta_m = \pi/2)$, with

$$\tilde{n}_e(\theta_m) = (\cos^2 \theta_m / n_o^2 + \sin^2 \theta_m / n_e^2)^{-1/2}. \quad (\text{B4})$$

By means of θ_m we “tune” the extraordinary index of refraction between n_o and n_e . The graphs of the indices of refraction shown in Fig. 10 correspond to those of the negative uniaxial beta-barium-borate crystal, with the index of refraction given by³⁴

$$n = \left[A + \frac{B}{\lambda^2 + C} + D\lambda^2 \right]^{1/2}, \quad (\text{B5})$$

where the constants for n_o and n_e are $A_o = 2.7359$, $B_o = 0.01878 \mu\text{m}^2$, $C_o = -0.01822 \mu\text{m}^2$, $D_o = -0.01354 \mu\text{m}^{-2}$ and $A_e = 2.3753$, $B_e = 0.01224 \mu\text{m}^2$, $C_e = -0.01667 \mu\text{m}^2$, and $D_e = -0.01516 \mu\text{m}^{-2}$. For beta-barium-borate we can verify that $n_o = 1.658$ at 915.8 nm and $n_e = 1.542$ at 457.9 nm. Under the situation known as type-I phase matching, the pump photon has the extraordinary in-

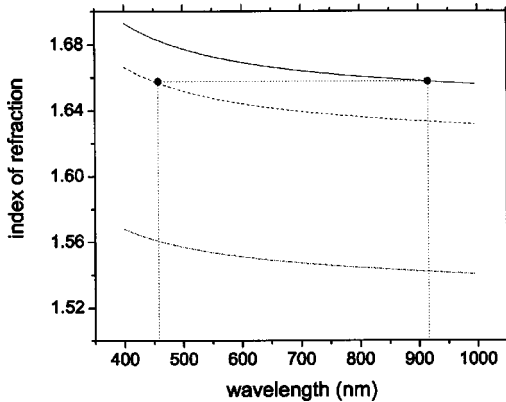


Fig. 10. Index of refraction curves for a beta-barium-borate crystal with its optic axis aligned perpendicular (top) and parallel (bottom) to the input polarization. The dashed middle curve corresponds to the phase-matching condition that allows down-conversion for the setup of Fig. 1(b).

dex of refraction $\tilde{n}_e(\theta_m)$ and the down-conversion photons have the ordinary index of refraction. Suppose that we wish to have the two down-conversion photons collinear, that is, $\theta_c = 0$ in Eq. (B3). Then by setting $\theta_m = 25.67^\circ$, the pump beam will have the index of refraction given by the dashed line in Fig. 10, or $n_p = \tilde{n}_e(\theta_m) = 1.658$ (at 457.9 nm). If we want the signal and idler beams to form a laboratory angle of $\theta_L = 3^\circ$ with the pump beam outside the crystal, we can use Snell’s law, $\sin \theta_L = n_s \sin \theta_c$, to obtain θ_c and find the phase matching angle θ_m that satisfies Eq. (B3).

¹*The Physics of Quantum Information*, edited by D. Bouwmeester, A. Ekert, and A. Zeilinger (Springer, Berlin, 2000).

²D. Dehlinger and M. W. Mitchell, “Entangled photon apparatus for the undergraduate laboratory,” *Am. J. Phys.* **70**, 898–902 (2002); *ibid.*, “Entangled photons, nonlocality, and Bell inequalities in the undergraduate laboratory,” *Am. J. Phys.* **70**, 903–910 (2002).

³C. H. Holbrow, E. J. Galvez, and M. E. Parks, “Photon quantum mechanics and beam splitters,” *Am. J. Phys.* **70**, 260–265 (2002).

⁴Richard P. Feynman, *QED, The Strange Theory of Light and Matter* (Princeton University Press, Princeton, 1985).

⁵S. Friedberg, C. K. Hong, and L. Mandel, “Measurement of time delays in the parametric production of photon pairs,” *Phys. Rev. Lett.* **54**, 2011–2013 (1985).

⁶Single Photon Counting Module SPCM-AQR Series, Perkin Elmer Optoelectronics product report (Perkin Elmer, Vaudreuil, 2001).

⁷Since we completed this work, the available power levels for the 400–410 nm diode lasers have risen to 50 mW. In addition, new diode lasers at 375 nm have become available.

⁸If the initial propagation direction is (1,0,0), with polarization along (0,0,1), then a sequence of mirrors that send the beam consecutively through the directions (0,0,1), (0,1,0), (1,0,0) rotates the polarization by 90° . Omitting the last step allows the same rotation when steering the beam into the (0,1,0) direction.

⁹For more information, see <<http://departments.colgate.edu/physics/pql.htm>>.

¹⁰R. P. Feynman, R. B. Leighton, and M. Sands, *The Feynman Lectures on Physics* (Addison-Wesley, Reading, 1965), Vol. 3, p. 1-1.

¹¹Note that $e^{ik\ell}$ is an example of Feynman’s formulation of quantum mechanics in terms of the action: $e^{i\int p dx/h}$. See R. P. Feynman, *The Theory of Fundamental Processes* (W. A. Benjamin, New York, 1962).

¹²We use $\delta_j = nk_j \ell_j \approx k_j \ell_j$ because $n \approx 1$ for experiments done in air.

¹³D. M. Greenberger, M. A. Horne, and A. Zeilinger, “Multiparticle interferometry and the superposition principle,” *Phys. Today* **46**(8), 22–29 (1993).

¹⁴In this case the $\pi/2$ relative phase between r and t yields $P(\delta) = 2RT[1 - \cos \delta]$.

¹⁵The pattern of the maxima and minima will be the same for tagged photons as for untagged photons. A tagged photon, however, is a special case of a biphoton which is discussed later, and its pattern of partial interference is not the same as that of an untagged photon.

¹⁶We fit the data using the “solver” option of Excel, minimizing the reduced χ^2 . The errors were calculated using the $\chi^2 + 1$ criterion. K. E. Schalm, “Least-squares fits to an arbitrary function using Excel,” (handout for PHY 445/PHY 515 Advanced Laboratory course at SUNY, Stony Brook, 9/18/95, unpublished).

¹⁷P. A. M. Dirac, *The Principles of Quantum Mechanics* (Clarendon Press, Oxford, 1958), p. 9.

¹⁸R. Ghosh, C. K. Hong, Z. Y. Ou, and L. Mandel, “Interference of two photons in parametric down conversion,” *Phys. Rev. A* **34**, 3962–3968 (1986).

¹⁹C. K. Hong, Z. Y. Ou, and L. Mandel, “Measurement of subpicosecond time intervals between two photons by interference,” *Phys. Rev. Lett.* **59**, 2044–2046 (1987).

²⁰P. G. Kwiat and R. Y. Chiao, “Observation of a nonclassical Berry’s phase for the photon,” *Phys. Rev. Lett.* **66**, 588–591 (1991).

²¹E. Mohler, J. Brendel, R. Lange, and W. Martienssen, “Finesse and resolution enhancement in two-photon interferometry,” *Europhys. Lett.* **8**, 511–516 (1989).

²²J. Brendel, E. Mohler, and W. Martienssen, “Time-resolved dual-beam two-photon interferences with high visibility,” *Phys. Rev. Lett.* **66**, 1142–1145 (1991).

- ²³Due to the better alignment and simpler optical arrangement that we can obtain in the experiment with collinear photons, the coincidence yield is much higher than in the experiments with the noncollinear photons.
- ²⁴Notice that the result is just the square of the result for one-photon interference. In other words, the interference pattern of the biphoton is the product of the interference patterns of single photons.
- ²⁵We detect coincidences at the interferometer output by placing a beam splitter there with reflectance R' and transmittance T' and then detecting coincidences between photons leaving each output. This arrangement allows us to detect only $2R'T'$ of the photon pairs leaving the interferometer.
- ²⁶R. A. Campos, B. E. A. Saleh, and M. A. Teich, "Fourth-order interference of joint single-photon wavepackets in lossless optical systems," *Phys. Rev. A* **42**, 4127–4137 (1990).
- ²⁷Roy J. Glauber, "Dirac's famous dictum on interference: One photon or two?," *Am. J. Phys.* **63**, 12(L) (1990). We thank H. Leff for bringing this reference to our attention.
- ²⁸P. D. D. Schwindt, P. G. Kwiat, and B.-G. Englert, "Quantitative wave-particle duality and nonerasing quantum erasure," *Phys. Rev. A* **60**, 4285–4290 (1999).
- ²⁹M. B. Schneider and I. A. LaPuma, "A simple experiment for discussion of quantum interference and which-way measurement," *Am. J. Phys.* **70**, 266–271 (2002).
- ³⁰C. H. Holbrow, J. N. Lloyd, and J. C. Amato, *Modern Introductory Physics* (Springer-Verlag, New York, 1999).
- ³¹G. Greenstein and A. G. Zajonc, *The Quantum Challenge* (Jones and Bartlett, Sudbury, 1987).
- ³²P. Grangier, G. Roger, and A. Aspect, "Experimental evidence for a photon anticorrelation effect on a beam splitter: A new light on single-photon interferences," *Europhys. Lett.* **1**, 173–179 (1986).
- ³³J. J. Thorn, M. S. Neel, V. W. Donato, G. S. Bergreen, R. E. Davies, and M. Beck, "Observing the quantum behavior of light in an undergraduate laboratory," *Am. J. Phys.* **72**, 1210–1219 (2004).
- ³⁴K. Kato, "Second harmonic generation of 2048 Å β -BaB₂O₄," *IEEE J. Quantum Electron.* **QE-22**, 1013–1014 (1986).

NEWTON'S BEQUEST

So gravity was not mechanical, not occult, not a hypothesis. He had provided it by mathematics. "It is enough," he said, "that gravity really exists and acts according to the laws that we have set forth and is sufficient to explain all the motions of the heavenly bodies and of our sea." It could not be denied, even if its essence could not be understood.

He had declared at the outset that his mission was to discover the forces of nature. He deduced forces from celestial bodies' motion, as observed and recorded. He made a great claim—the System of the World—and yet declared his program incomplete. In fact, incompleteness was its greatest virtue. He bequeathed to science, that institution in its throes of birth, a research program, practical and open-ended. There was work to do, predictions to be computed and then verified.

James Gleick, *Isaac Newton* (Vintage Books, 2003), pp. 139–140.